*Proc. Natl. Acad. Sci. USA*
Vol. 82, pp. 401–405, January 1985
Biophysics

# Imaging of optically active biological structures by use of circularly polarized light

**(microscopy/circular dichroism/circular intensity differential scattering)**

DAVID KELLER‡§, CARLOS BUSTAMANTE¶, MARCOS F. MAESTRE||, AND IGNACIO TINOCO, JR.‡

‡Department of Chemistry and Laboratory of Chemical Biodynamics, University of California, Berkeley, CA 94720; ¶Department of Chemistry, University of New Mexico, Albuquerque, NM 87131; ||Lawrence Berkeley Laboratory, Division of Biology and Medicine, University of California, Berkeley, CA 94720

*Communicated by Harden M. McConnell, September 19, 1984*

**ABSTRACT** **If an optically active (chiral) sample is placed in a microscope and illuminated with circularly polarized light, an image can be formed that is related to the circular dichroism of each feature of the sample. A theoretical investigation has been done for the circular differential image obtained by subtracting the images formed under right- and left-circularly polarized light. Two types of differential images are possible: (*i*) dark-field images formed from light reflected or scattered by the sample and (*ii*) bright-field images formed from light transmitted through the sample. The sign and magnitude of each feature in a circular differential image strongly depend on the structure of the sample. The dark-field circular differential images are most sensitive to large features with dimensions similar to the wavelength of illumination whereas the bright-field images are most sensitive to the short-range molecular order. Applications of circular differential imaging may include clinical fingerprinting of normal and transformed cells and structural analysis of individual cellular components.**

Chiral objects interact differently with right- and left-circularly polarized light. The ability of certain substances to transmit the two circularly polarized lights with different speeds is known as optical rotatory dispersion (ORD) and the ability to absorb different amounts of the two is known as circular dichroism (CD). These phenomena constitute what traditionally has been called optical activity. More recently, it has been established that chiral objects also have the ability to scatter different amounts of right- and left-circularly polarized light (1–5). It is possible to measure the difference in the scattered light intensity at each direction in space when right- and left-circularly polarized light are incident on the sample. The resulting difference scattering pattern has been termed circular intensity differential scattering (CIDS). It has also been shown that the circular intensity differential scattering can give rise to an apparent circular dichroism (6).

The relationship between the chirality of the illuminated object and the handedness of the incident light makes techniques based on optical activity very sensitive to changes in the structure of the object.

If an imaging system (a lens or a microscope) is placed between the chiral sample and the detector, an image can be formed. The image produced by left-circularly polarized illumination will be different from the image produced when the illumination is right-circularly polarized. The difference between these two images is called a circular differential image. The information contained in a circular differential image will not be the same as the information in an image produced using unpolarized light. In the latter case, the optical contrast that distinguishes one feature of the sample from another is provided by differences in the absorption and index of refraction of various parts of the sample. In a circular differential image, the contrast is provided by differences in the interaction of different parts of the sample with left- and right-circularly polarized light.

It will be shown below that the intensity of each feature in a circular differential image is proportional to the "optical activity" of that feature in the particular direction from which the sample is being viewed. This optical activity may take the form of circular dichroism or circular intensity differential scattering and contains information on the chiral structure of each feature. This structural sensitivity is perhaps the most important property of circular differential imaging. For example, circular differential imaging can be used to follow the organization of a chromosome as a function of the cell cycle and obtain information on the super-organization of chromatin. In clinical applications it may be possible to correlate the circular differential imaging pattern of a cell with the type of cell, the stage of the cell cycle, and whether the cell is normal or transformed (neoplastic). That is, a circular differential image can be used as a fingerprint of the state of the cell.

## THEORY

Consider a sample made up of a collection of small groups that are capable of interacting with the incident illumination. The scattering and absorptive properties of each group can then be described by a polarizability tensor, $\boldsymbol{\alpha}$. Some of the optical activity of the sample will result from the intrinsic properties of each individual group, and this information is contained in the polarizability tensors associated with the groups. This optical activity is due to the short-range structure of the sample and is manifested primarily as circular dichroism. The remainder of the optical activity arises from the long-range spatial organization of the collection of groups as a whole and is manifested primarily in the circular intensity differential scattering.

After the light has interacted with the sample, two qualitatively different imaging experiments are possible: (*a*) Bright-field imaging, in which the microscope and detector are placed directly behind the sample. (*b*) Dark-field imaging, in which the microscope and detector are placed at an angle to the incident beam. Fig. 1 shows the experimental geometry.

We present here a brief derivation of the major results of the theory. A detailed discussion will be published elsewhere. The image calculation has been treated in the following way.

(*i*) The electric field scattered or transmitted by the sample is calculated using classical scattering theory (3, 7–9). For the dark-field experiment, $\mathbf{E}(\mathbf{r}')$ is the field scattered by

The publication costs of this article were defrayed in part by page charge payment. This article must therefore be hereby marked "*advertisement*" in accordance with 18 U.S.C. §1734 solely to indicate this fact.

§Present address: Department of Chemistry, University of New Mexico, Albuquerque, NM 87131.

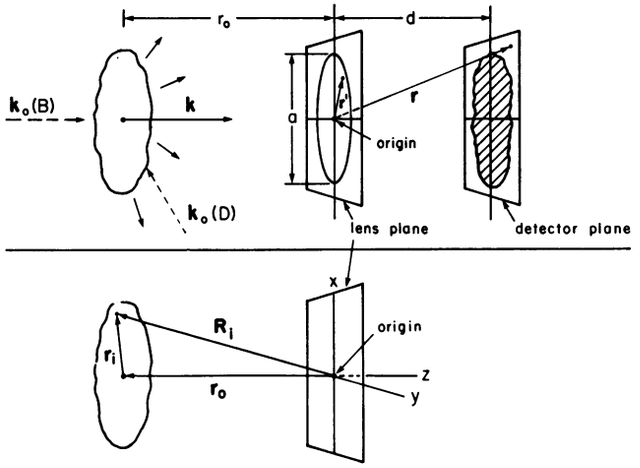


FIG. 1. Geometry for the differential imaging calculations. (*Upper*) The vectors $\mathbf{k}_0$ show the direction of the incident light for the bright-field (B) and dark-field (D) experiments. The other variables are the distance between the sample and the lens, $r_0$; the distance between the lens and the detector screen, $d$; the lens aperture diameter, $a$; the direction of propagation of the scattered light, $\mathbf{k}$; the position in the lens plane, $\mathbf{r}'$; and the position in the detector screen plane, $\mathbf{r}$. (*Lower*) Variables used in describing the relation between the sample and the imaging system are shown.

the sample (5):

$$\mathbf{E}(\mathbf{r}') = \mathbf{E}_{\text{scatt}}(\mathbf{r}') = \frac{k^2 e^{ikr_0}}{r_0} e^{ik(\mathbf{r}')^2/2r_0}(1 - \hat{\mathbf{k}}\hat{\mathbf{k}}) \cdot \sum e^{-ik(\mathbf{r}'-\mathbf{r}_0)\cdot\mathbf{r}_i/r_0}\boldsymbol{\alpha}_i \cdot \hat{\boldsymbol{\varepsilon}}_0 E_0 e^{i\mathbf{k}_0\cdot(\mathbf{r}_i+\mathbf{r}_0)}, \quad [1]$$

where $k = 2\pi/\lambda$ is the wavenumber of the incident light, $\mathbf{r}'$ is a position vector in the lens plane, $r_0$ is the distance between the sample and the lens plane, $\hat{\mathbf{k}}$ is a unit vector pointing from the center of the lens toward the sample, $\mathbf{r}_0$ is the vector from the sample to the center of the lens, $\mathbf{r}_i = \mathbf{R}_i - \mathbf{r}_0$ [where $\mathbf{R}_i$ is the vector pointing from the center of the lens to the $i$th group (see Fig. 1)], $\boldsymbol{\alpha}_i$ is the polarizability tensor of the $i$th group, and $E_0$, $\hat{\boldsymbol{\varepsilon}}$, and $\mathbf{k}_0$ are the amplitude, polarization, and wavevector of the incident light. In Eq. **1**, we have assumed that the lens aperture and the dimensions of the sample are much smaller than the distance $r_0$ between the scatterer and the lens. Also, the field in Eq. **1** is computed in the first Born approximation—that is, we have assumed that there is no appreciable induced-dipole–induced-dipole interaction between groups or multiple scattering in the sample. Some of the effects of dipole–dipole interactions and multiple scattering can be taken into account by the use of the second Born approximation. This amounts to replacing $\boldsymbol{\alpha}_i$ in Eq. **1** with an effective polarizability that contains the coupling information (7, 10). Higher-order terms of the Born series can be treated in a similar way.

For the bright-field experiment, the electric field at the near face of the lens includes both incident and scattered waves:

$$\mathbf{E}(\mathbf{r}') = E_0\hat{\boldsymbol{\varepsilon}}_0 e^{i\mathbf{k}_0\cdot\mathbf{r}'} + \mathbf{E}_{\text{scatt}}(\mathbf{r}'). \quad [2]$$

(*ii*) We take the imaging apparatus to be a single thin lens. That is, after the scattered or transmitted light has left the sample and arrived at the lens, the effect of the imaging system is to modulate the phase of the field as a function of position in the lens plane, while the polarization and magnitude of the field are not altered at all. Specifically, we take the electric field on the far face of the lens (after passing through the lens, but before beginning to propagate toward the detector screen) to be

$$\mathbf{E}_f(\mathbf{r}') = e^{i\phi(\mathbf{r}')}\mathbf{E}(\mathbf{r}'), \quad [3]$$

where $\mathbf{E}_f$ and $\mathbf{E}$ are the electric fields on the far and near faces, respectively, and $\mathbf{r}'$ is a position vector in the lens plane (see Fig. 1). The phase function $\phi(\mathbf{r}')$ is given by (7)

$$\phi(\mathbf{r}') = kn\Delta_0 - k(\mathbf{r}')^2/2f, \quad [4]$$

where $k = 2\pi/\lambda$ is the wavenumber of the incident light, $n$ is the index of refraction of the lens material, $\Delta_0$ is the thickness of the lens at its widest point, $(\mathbf{r}')^2 = |\mathbf{r}'|^2$, and $f$ is the focal length of the lens. It can be shown (11) that a lens with these properties behaves according to geometrical optics. We have therefore chosen the simplest possible image-forming device for the purpose of investigating the general properties of circular differential images. The theory can be extended in principle to large-aperture lenses (12). However, it is important that the imaging system be insensitive to the polarization of the scattered light.

(*iii*) Once the electric field is known on the lens, we calculate the propagation of the field outward from the lens toward the detector screen by using vector diffraction theory in the Fresnel limit (13). It is customary in thin-lens calculations to use scalar diffraction theory at this point. However, here we are interested specifically in effects caused by the polarization of light, and so vector diffraction theory is appropriate.

If the lens aperture $a$ is small compared to the distance $d$ between the detector screen and the lens plane (see Fig. 1), the electric field on the detector plane is given by (13)

$$\mathbf{E}(\mathbf{r}) = \frac{ie^{ikr}}{2\pi r} k\hat{\mathbf{r}} \times \left[\int_{\text{aperture}} \hat{\mathbf{n}} \times \mathbf{E}_f(\mathbf{r}')\exp\left(-ik\hat{\mathbf{r}}\cdot\mathbf{r}' + \frac{ik(\mathbf{r}')^2}{2r}\right)dS\right], \quad [5]$$

where $\mathbf{r}$ is a position vector pointing from the center of the lens to a spot in the detector plane, $r = |\mathbf{r}|$, $\hat{\mathbf{r}} = \mathbf{r}/r$, and $\hat{\mathbf{n}}$ is a unit vector normal to the surface of the lens plane. The integration in Eq. **5** is over the surface of the lens aperture. We choose the lens and detector planes to be parallel to the $xy$ plane, so that the unit vector normal to the surface, $\hat{\mathbf{n}}$, is along the $z$ axis.

**Dark-Field Circular Differential Imaging.** All parts of the calculation are now specified. To obtain the image electric field (i.e., the field arriving at the detector) in the dark-field case, we substitute Eqs. **1**, **3**, and **4** into Eq. **5**:

$$\mathbf{E}(\mathbf{r}) = C\sum_i F(\mathbf{k},\mathbf{r}_i)e^{-i\Delta\mathbf{k}\cdot\mathbf{r}_i}\hat{\mathbf{r}} \times [\hat{\mathbf{k}} \times (\boldsymbol{\alpha}_i \cdot \hat{\boldsymbol{\varepsilon}}_0)], \quad [6]$$

where $\Delta\mathbf{k} = \mathbf{k} - \mathbf{k}_0$ is the momentum-transfer vector for scattering in the $\mathbf{k}$ direction,

$$C = \frac{iE_0k^3 \cdot \exp[i(kn\Delta_0 + \mathbf{k}_0\cdot\mathbf{r}_0 + kr + kr_0)]}{2\pi r r_0},$$

and $F(\mathbf{k},\mathbf{r}_i)$ is given by

$$F(\mathbf{k},\mathbf{r}_i) = \int_{\text{aperture}} \exp\left[\frac{ik}{2}\left(\frac{1}{r_0} + \frac{1}{r} - \frac{1}{f}\right)(\mathbf{r}')^2 - i\left(\mathbf{k} + \frac{k\mathbf{r}_i}{r_0}\right)\cdot\mathbf{r}'\right]dS. \quad [7]$$

The integral in Eq. 7 is commonly found in imaging theories based on scalar diffraction theory. It is this integral that gives the localized field intensity that will produce an image of the scattering sample. In Eq. 7 the quantity $1/r_0 + 1/r - 1/f$ appears. According to geometric optics, the condition for a thin lens to produce a focused image is $1/r_0 + 1/d - 1/f = 0$, where $d$ is the distance from the lens plane to the detector plane (see Fig. 1). For points in the detector plane near the lens axis, $d \approx r$, and we may set the first term in the argument of the exponential in Eq. 7 equal to zero. The second term in the exponential can be rewritten in terms of the magnification of the imaging system:

$$\left(\mathbf{k} + \frac{k\mathbf{r}_i}{r_0}\right) \cdot \mathbf{r}' = \frac{k}{r}\,[(x + mx_i)^2 + (y + my_i)^2]^{1/2} r' \cos\phi\,(\mathbf{r}'),$$

where $x_i$ and $y_i$ are the $x$ and $y$ components of $\mathbf{r}_i$, $x$ and $y$ are the $x$ and $y$ components of $\mathbf{r}$, and $m = r/r_0$ is the lens magnification. The remaining integration may be performed directly:

$$F(\mathbf{k},\mathbf{r}_i) = F(\rho_i) = 2\pi a^2 \left[\frac{J_1\left(\frac{2\pi}{\Lambda}\rho_i\right)}{\frac{2\pi}{\Lambda}\rho_i}\right], \qquad [8]$$

where $J_1$ is the Bessel function of the first kind of order 1, $\rho_i = [(x + mx_i)^2 + (y + my_i)^2]^{1/2}$ and $\Lambda/\lambda = (m + 1)f/a$. The function $F(\rho_i)$ reaches a maximum when $\rho_i = 0$ (that is, when $x = -mx_i$ and $y = -my_i$) and diminishes for all nonzero values of $\rho_i$.

To calculate the dark-field circular differential image, we must calculate the image intensity at the detector for right- and left-circularly polarized illumination and then subtract. To do this, we substitute left- and right-circular polarization vectors for the incident polarization vector $\hat{\boldsymbol{\varepsilon}}_0$ in Eqs. 5 and 6 and square the electric field to obtain left- and right-circular intensities. The unit vectors for left- and right-circular polarization are

$$\hat{\boldsymbol{\varepsilon}}_L = \frac{1}{\sqrt{2}}(\hat{\boldsymbol{\varepsilon}}_1 + i\hat{\boldsymbol{\varepsilon}}_2) \text{ and } \hat{\boldsymbol{\varepsilon}}_R = \frac{1}{\sqrt{2}}(\hat{\boldsymbol{\varepsilon}}_1 - i\hat{\boldsymbol{\varepsilon}}_2), \qquad [9]$$

respectively, where $\hat{\boldsymbol{\varepsilon}}_1$, $\hat{\boldsymbol{\varepsilon}}_2$, and $\hat{\mathbf{k}}_0$ form a right-handed orthogonal coordinate frame. After some algebra, we obtain

$$I_L - I_R = |C|^2 \sum_{i \le j}\sum F(\rho_i)F(\rho_j)\,\Delta I_{ij}\,(\mathbf{k},\mathbf{k}_0), \qquad [10]$$

where the differential intensity $\Delta I_{ij}$ is given by

$$\Delta I_{ij}\,(\mathbf{k},\mathbf{k}_0) = I_{ijL} - I_{ijR},$$

with

$$I_{ijL,R} = 2\mathrm{Re}\,\{e^{-i\Delta\mathbf{k}\cdot\mathbf{r}_{ij}}\hat{\boldsymbol{\varepsilon}}^*_{L,R} \cdot \boldsymbol{\alpha}^\dagger \cdot (1 - \hat{\mathbf{k}}\hat{\mathbf{k}}) \cdot \boldsymbol{\alpha} \cdot \boldsymbol{\varepsilon}_{L,R}\} \quad [11]$$

and $\mathbf{r}_{ij} = \mathbf{r}_j - \mathbf{r}_i \cdot \boldsymbol{\alpha}_i^\dagger$ is the Hermitian conjugate of $\boldsymbol{\alpha}_i$ (i.e., $[\boldsymbol{\alpha}^\dagger]_{mn} = [\boldsymbol{\alpha}_i]^*_{nm}$). In arriving at Eq. 11, we have taken $\hat{\mathbf{r}} \approx \hat{\mathbf{k}}$, which is valid for images in the portion of the detector screen close to the lens axis.

The differential intensity $\Delta I_{ij}(\mathbf{k},\mathbf{k}_0)$ is the scattering optical activity of the sample in the $\mathbf{k}$ direction due to the pair of groups $i$ and $j$ (7, 10, 14). That is, if the two groups bear a chiral geometrical relationship to each other, then $\Delta I_{ij}$ is the difference in the light intensity scattered in the direction of view when the incident light is left- and right-circularly polarized. In the case where $i = j$, $\Delta I_{ij}$ is the difference in the left and right intensities scattered by a single group. The pairwise differential intensities $\Delta I_{ij}$ $(i \neq j)$ arise due to interference between image fields for the groups $i$ and $j$ and correspond to the interference fringes that occur in ordinary light microscopy. For groups that are well resolved from each other, these pairwise differential intensities do not contribute. The self-differential intensities, $\Delta I_{ii}$, arise from the intrinsic optical activity of each individual group and correspond to well-resolved image points in ordinary microscopy. The chief result of our theory then is that the circular differential image is composed of a collection of image spots and interference fringes much like an image produced with unpolarized light, except that in the circular differential image each feature has an apparent intensity proportional to the circular differential intensity $\Delta I_{ij}$ (which may be positive or negative) instead of the total intensity, $I_{ij} = I_{ijL} + I_{ijR}$.

To illustrate these properties, we have used the expressions derived above to calculate dark-field circular differential images of the three helices shown in Fig. 2. Two of the helices are the same size and have the same orientation with respect to the incident light but have opposite handedness. The third helix is right-handed and smaller by a factor of 3. Fig. 3 compares the circular differential image with the usual image. The light is incident from the bottom of Fig. 3 toward the top, and the point of view is from directly above at 90° to the direction of incidence. The incident wavelength is equal to one-tenth the pitch of the large helices. The differential images of the two large helices are roughly equal in shape and size but opposite in sign; this indicates that the helices have opposite handedness. The usual image does not reveal the sense of the helix. We have used a very short wavelength to make up for the low resolution required by the approximations in the theory.

**Bright-Field Circular Differential Imaging.** In the previous discussion, we considered dark-field circular differential imaging, in which the sample is viewed at an angle to the incident illumination. When the lens and detector are placed di-

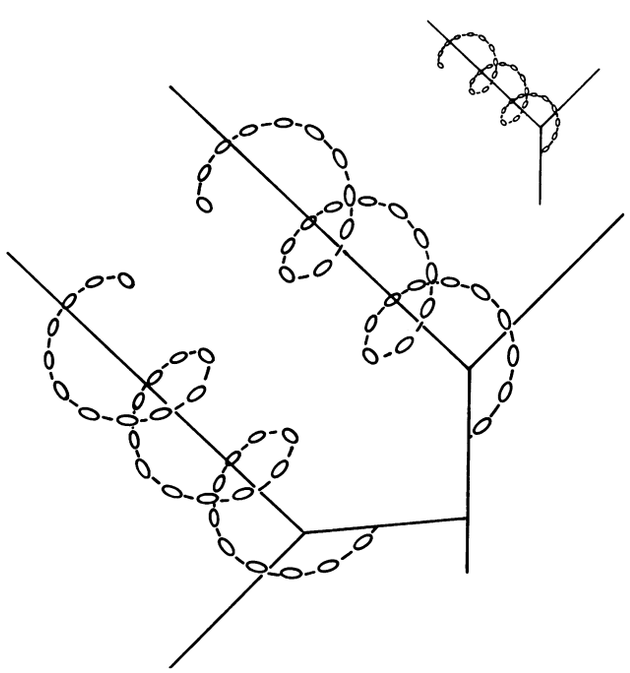

FIG. 2. Three helices. The two large helices are equal in size (pitch = 600 nm, radius = 300 nm, 3 turns long) but have opposite handedness. The helix on the left is left-handed, and the helix on the right is right-handed. The small helix has a pitch of 200 nm and radius of 100 nm and is also 3 turns long.

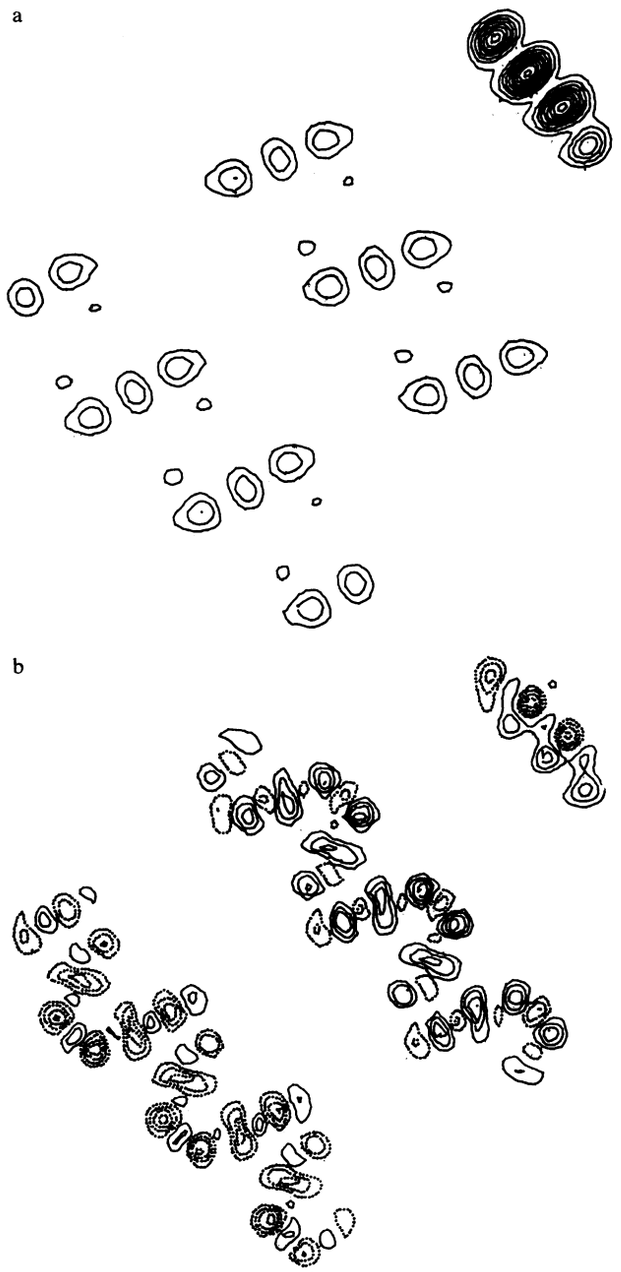


FIG. 3. Images of the helices in Fig. 2. (*a*) Normal image. (*b*) Circular differential image. In both images, the light is incident from the bottom and the point of view is from above, at 90° to the direction of incidence. The aperture $a$, focal length $f$, and magnification $m$ of the lens have been chosen so that the resolution length, $\Lambda = (m + 1)f\lambda/a$, is equal to $4\lambda$. The incident wavelength is 60 nm; the maximum differential intensity is about 0.3 times as large as the total image intensity. The small helix image intensities have been divided by 5 to facilitate plotting. Continuous contours indicate positive values of the circular differential image whereas dotted contours indicate negative values.

rectly behind the sample, the electric field arriving at the lens plane has two parts: the forward-scattered electric field and the incident electric field. In classical electrodynamics it is the interference between these two fields that leads to absorptive effects. The primary difference between the bright-field and dark-field differential imaging experiments is the presence of these absorptive effects in the bright-field image.

When Eq. 2 for the electric field at the near face of the lens is substituted into Eqs. 3 and 5, two image fields will result—one originating from the incident field and one originating from the scattered field:

$$\mathbf{E}(\mathbf{r},\hat{\boldsymbol{\varepsilon}}_0) = \mathbf{E}_I(\mathbf{r},\hat{\boldsymbol{\varepsilon}}_0) + \mathbf{E}_S(\mathbf{r},\hat{\boldsymbol{\varepsilon}}_0), \qquad [12]$$

where $\hat{\boldsymbol{\varepsilon}}$ is the incident polarization, $\mathbf{E}$ is the total image field, $\mathbf{E}_I$ is the image field due to the incident light, and $\mathbf{E}_S$ is the image field due to the forward-scattered light (given by Eq. 6 with $\mathbf{k} = \mathbf{k}_0$). The field $\mathbf{E}_I$ is given by

$$\mathbf{E}_I(\mathbf{r},\hat{\boldsymbol{\varepsilon}}_0) = C'\hat{\mathbf{r}} \times (\hat{\mathbf{k}}_0 \times \hat{\boldsymbol{\varepsilon}}_0) \int_{\text{aperture}} \exp\left[\frac{ik}{2}\left(\frac{1}{r} - \frac{1}{f}\right)\mathbf{r}' - i(k\mathbf{r} - \mathbf{k}_0)\cdot\mathbf{r}'\right] dS, \qquad [13]$$

where

$$C' = \frac{ie^{ikr}}{2\pi r} k\mathbf{E}_0 e^{ikn\Delta_0}.$$

If the lens aperture has a finite diameter, the integration in Eq. 13 is very difficult. However, this field is the one that provides the bright background illumination in a bright-field experiment, and, therefore, we expect it to be very slowly varying over the surface of the detector screen. The smaller the aperture the more slowly varying the background field is. It can be shown that even if the aperture is taken to be infinite, $\mathbf{E}_I$ is still approximately constant for the portion of the detector screen near the lens axis. For an infinite aperture, then, Eq. 13 becomes

$$\mathbf{E}_I(\mathbf{r},\hat{\boldsymbol{\varepsilon}}_0) = C'\hat{\mathbf{r}} \times (\hat{\mathbf{k}}_0 \times \hat{\boldsymbol{\varepsilon}}_0)\left(\frac{-2\pi i r_0}{k}\right) \exp\left[\frac{ir_0 k}{2r^2}(x^2 + y^2)\right] \approx C'\hat{\boldsymbol{\varepsilon}}_0\left(\frac{2\pi i r_0}{k}\right), \qquad [14]$$

where we have used $1/r - 1/f = 1/r_0$, and the second equation holds for portions of the detector screen near the lens axis ($\hat{\mathbf{r}} \approx \hat{\mathbf{k}}_0$).

To find the bright-field differential image we square Eq. 12 with $\hat{\boldsymbol{\varepsilon}}_0 = \hat{\boldsymbol{\varepsilon}}_L$ or $\hat{\boldsymbol{\varepsilon}}_R$ (as defined in Eq. 9) and subtract:

$$I_L - I_R = (I_L - I_R)_I + 2\text{Re}\{\mathbf{E}_I(\mathbf{r},\hat{\boldsymbol{\varepsilon}}_L)\cdot\mathbf{E}_S^*(\mathbf{r},\boldsymbol{\varepsilon}_L) - \mathbf{E}_I(\mathbf{r},\hat{\boldsymbol{\varepsilon}}_R)\cdot\mathbf{E}_S^*(\mathbf{r},\hat{\boldsymbol{\varepsilon}}_R)\} + (I_L - I_R)_S, \qquad [15]$$

where

$$(I_L - I_R)_I = |\mathbf{E}_I(\mathbf{r},\hat{\boldsymbol{\varepsilon}}_L)|^2 - |\mathbf{E}_I(\mathbf{r},\hat{\boldsymbol{\varepsilon}}_R)|^2 = 0,$$

and

$$(I_L - I_R)_S = |\mathbf{E}_S(\mathbf{r},\hat{\boldsymbol{\varepsilon}}_L)|^2 - |\mathbf{E}_S(\mathbf{r},\hat{\boldsymbol{\varepsilon}}_R)|^2.$$

The quantity $(I_L - I_R)_I$, the background illumination, does not contribute to the differential image. The quantity $(I_L - I_R)_S$ is just the dark-field differential image evaluated for scattering in the forward direction and has already been discussed. The remaining terms in Eq. 15 contain the absorptive effects. Usually the incident field is much larger than the scattered field, and so these absorption terms should give the primary contributions to the bright-field image. In the first Born approximation, the forward-scattered light cannot

contribute at all to the differential image, and $(I_L - I_R)_S = 0$. Substituting Eqs. **6** and **14** into Eq. **15**, we obtain for the absorption terms which dominate the circular differential image:

$$\text{CDI} = -K\sum_i F(\rho_i)\Delta I_i^{\text{abs}}, \qquad [16]$$

where

$$\Delta I_i^{\text{abs}} = I_{iL}^{\text{abs}} - I_{iR}^{\text{abs}},$$

$$\text{with } I_{iL,R}^{\text{abs}} = Im(\hat{\boldsymbol{\epsilon}}_{L,R}^* \cdot \boldsymbol{\alpha}_i \cdot \hat{\boldsymbol{\epsilon}}_{L,R}) \text{ and } K = \frac{|E_0|^2 k^3}{2\pi r^2}.$$

$\Delta I_i^{\text{abs}}$ is proportional to the difference in the absorbed intensities for left- and right-circularly polarized light. The minus sign in front of the right-hand side of Eq. **16** is due to the fact that the transmitted intensity $I_L$ or $I_R$ in Eq. **15** is equal to the incident intensity *minus* the absorbed intensity: $I_{L,R} = I_{0L,R} - I_{L,R}^{\text{abs}}$ (in the absence of any appreciable forward scattering).

It can be shown that at the position of a well-resolved feature the bright-field circular differential image reduces to approximately the circular dichroism of the feature. In the bright-field experiment, therefore, the circular differential image is essentially a map of the circular dichroism of each feature of the sample.

Usually the circular dichroism is sensitive to molecular structures of size on the order of a few tens of angstroms (6). The differential image in the bright-field case will therefore mainly contain information on short-range structure in the sample. However, if the sample is capable of appreciable scattering, the difference in total scattering cross-sections for left- and right-circularly polarized light can also contribute to the apparent circular dichroism. This contribution is largest when the dimensions of the scatterer are of the order of the incident wavelength. For incident wavelengths outside the absorption bands of the groups, only the differential scattering effects contribute to the circular dichroism. Inside the absorption bands, the absorptive circular dichroism is usually dominant, though the scattering contribution also increases as the absorption bands are approached (6).

## SUMMARY AND DISCUSSION

The circular differential image can be thought of as a two-dimensional mapping of the optical activity of the sample. Each feature in the image is differentiated from surrounding features by the differences in its optical activity rather than by differences in absorption or refractive index. This has two advantages. First, samples that have little or no contrast in an ordinary optical image may show contrast in a differential image. In effect, areas of differing structure and conformation are "stained" by their differing optical-activity properties. Second, the sign and magnitude of the optical activity of each feature are characteristic of structural properties that are too small to be resolved by the microscope directly. This should be especially valuable for parts of the system whose structure changes with time or environment: for example, the folding and unfolding of chromatin.

The optical activity of each feature in the sample manifests itself differently at different angles of observation with respect to the incident light and at different wavelengths of light. When the sample is viewed from directly opposite the source of illumination (bright-field experiment), the optical activity is primarily circular dichroism and is sensitive mainly to short-range molecular structure when the incident wavelength is inside the absorption bands. When the sample is viewed at an angle to the illuminating beam (dark-field experiment), the optical activity is due to circular differential scattering and is sensitive mainly to structures with dimensions similar to the incident wavelength. In the visible and UV regions this means very long-range macromolecular structure of dimensions on the order of thousands of angstroms.

In the previous discussion, we have considered only thin samples (that is, samples thin compared to the depth of field of the imaging device but not necessarily two-dimensional). Indeed, the form we have used for the scattered field (Eq. **1**) implies that all parts of the sample are in focus simultaneously. This has been adequate for our purposes here, but it is worth pointing out that contributions to the image from out-of-focus parts of the sample can be naturally accounted for in the theory by adding extra electric fields to the scattered field with the same form as in Eq. **1**, but with different values of the distance $r_0$ between a particular part of the sample and the lens. The images from these extra fields will not satisfy the thin lens equation, $1/r + 1/r_0 = 1/f$, and so will not be in focus, but they will contribute to the differential image. In this respect then, the differential image is quite similar to the normal image, and sectioning and Fourier-transform image-analysis techniques should be applicable.

This work was supported in part by National Institutes of Health Grants GM10840 (I.T.), AI08247 (M.F.M.), and GM32543 (C.B.), and by the U.S. Department of Energy, Office of Energy Research Contract DE-ATO3-82-ER60090. Additional support has been provided by a Searle Scholarship granted to one of the authors (C.B.).

1. Barron, L. D. & Buckingham, A. D. (1971) *Mol. Phys.* **20,** 1111–1119.
2. Harris, R. A., McClain, W. M. & Sloane, C. F. (1974) *Mol. Phys.* **28,** 381–398.
3. Bustamante, C., Maestre, M. F. & Tinoco, I., Jr. (1980) *J. Chem. Phys.* **73,** 4273–4281.
4. Bustamante, C., Maestre, M. F. & Tinoco, I., Jr. (1980) *J. Chem. Phys.* **73,** 6046–6055.
5. Bustamante, C., Tinoco, I., Jr., & Maestre, M. F. (1982) *J. Chem. Phys.* **76,** 3440–3446.
6. Bustamante, C., Tinoco, I., Jr., & Maestre, J. F. (1983) *Proc. Natl. Acad. Sci. USA* **80,** 3568–3572.
7. Keller, D. (1984) Dissertation (Univ. of California, Berkeley).
8. Saxon, D. S. (1955) *Lectures on the Scattering of Light*, Scientific Report No. 9, Contract AF19(122)-239, (Dept. Meteorol., Univ. of California, Los Angeles), pp. 38–73.
9. Bustamante, C. (1981) Dissertation (Univ. of California, Berkeley).
10. Bustamante, C., Maestre, M. F., Keller, D. & Tinoco, I., Jr. (1984) *J. Chem. Phys.* **80,** 4817–4823.
11. Goodman, J. W. (1968) *Introduction to Fourier Optics* (McGraw-Hill, San Francisco), pp. 77–80.
12. Born, M. & Wolf, E. *Principles of Optics* (Pergamon, Oxford), 6th Ed.
13. Jackson, J. D. (1975) *Classical Electrodynamics* (Wiley, New York), 2nd Ed., pp. 441–442.
14. Keller, D., Bustamante, C. & Tinoco, I., Jr. (1984) *J. Chem. Phys.* **81,** 1643–1649.